PHYSICAL REVIEW D **88,** 072007 (2013)

Experimental investigation of the Landau-Pomeranchuk-Migdal effect in low-Z targets

K. K. Andersen,[1] S. L. Andersen,[1] J. Esberg,[2] H. Knudsen,[1] R. E. Mikkelsen,[1] U. I. Uggerhøj,[1,*]
T. N. Wistisen,[1] P. Sona,[3] A. Mangiarotti,[4] and T. J. Ketel[5]

(CERN NA63 Collaboration)

[1]*Department of Physics and Astronomy, Aarhus University, 8000 Aarhus C, Denmark*
[2]*CERN, CH-1211 Geneva 23, Switzerland*
[3]*University of Florence, 50121 Florence, Italy*
[4]*University of São Paulo, 05508-060 São Paulo, Brazil*
[5]*Free University, 1081 HV Amsterdam, The Netherlands*
(Received 23 September 2013; published 15 October 2013)

In the CERN NA63 Collaboration we address the question of the potential inadequacy of the commonly used Migdal formulation of the Landau-Pomeranchuk-Migdal (LPM) effect by measuring the photon emission by 20 and 178 GeV electrons in the range of 100 MeV–4 GeV, in targets of low-density polyethylene, C, Al, Ti, Fe, Cu, Mo, and, as a reference target, Ta. For each target and energy, a comparison between simulated values based on the LPM suppression of incoherent bremsstrahlung is shown, taking multiphoton effects into account. For these targets and energies, we find that Migdal's theoretical formulation is adequate to a precision of better than about 5%, irrespective of the target substance.

DOI: 10.1103/PhysRevD.88.072007 PACS numbers: 13.40.−f, 12.20.Fv, 41.60.−m

I. INTRODUCTION

The well-known Landau-Pomeranchuk-Migdal (LPM) effect, which reduces the radiation emission from an ultrarelativistic electron in a medium due to multiple Coulomb scattering, has been investigated extensively at both SLAC and CERN. Nevertheless, the question remains if the ''traditional'' approach of using Migdal's theoretical formulation is adequate in the case of targets of low nuclear charge. Since the LPM effect is routinely applied in codes used to interpret extended air showers which naturally occur in a low-Z medium, the answer to this question is important. There is reason to suspect a certain degree of inadequacy since Migdal applied the Thomas-Fermi approach to determine the screening [[1] Eq. (22)], an approach that is inherently statistical and therefore inaccurate for atoms with few electrons, see e.g. [2]. As essentially all experiments are performed in the full-screening limit, the inaccuracy of the screening model might lead to imprecise answers. Furthermore, the contribution from electrons may be influenced differently by the LPM effect than by the nuclear contribution since a different range of momentum transfers are relevant and different screening parameters are involved [3]. And, finally, seemingly unphysical ''kinks'' in the calculated spectra based on Migdal's formulation appear when the Migdal formula reaches the Bethe-Heitler (BH) level.

Numerous previous experiments have presented evidence for the LPM effect, see e.g. [4], in particular the SLAC experiment performed with 8 and 25 GeV electrons [5,6], and the experiments at energies up to 287 GeV performed at CERN [7,8].

II. EXPERIMENT

The present experiment was performed in the H4 beam line in the North Experimental Area of the CERN Super Proton Synchrotron with tertiary beams of electrons with energies of 20 and 178 GeV. The 20 GeV beam was chosen to investigate experimentally the ''kink'' in the radiation spectrum obtained from Migdal's formula. The high energy was chosen to maximize the photon formation length given by $l_f = 2\gamma^2 c/\omega$ associated to the emission of photons with energies in the sensitive range of the bismuth germanate (BGO) calorimeter used, while retaining an acceptable beam intensity. Here γ is the Lorentz factor of the electron, c the speed of light, and ω the photon frequency.

A schematic drawing of the setup is shown in Fig. 1. The electron beam was defined by the scintillator counters S1, S2, $\overline{\text{S3}}$, where the latter is a Ø9 mm hole scintillator (used as a veto). The beam chosen in this way is centered on the target, and, after having traversed this, the electrons are swept away by two dipole magnets connected in series. This method of separation inevitably introduces synchrotron radiation (SR), the implication of which will be discussed below. To be able to correct for the background, an empty target run was performed. Vacuum pipes were used when possible to reduce background to a minimum in the 70 m long setup. The beam spot size at the calorimeter position was determined by scanning a 5 mm wide scintillator counter in the vertical and horizontal directions in

*ulrik@phys.au.dk

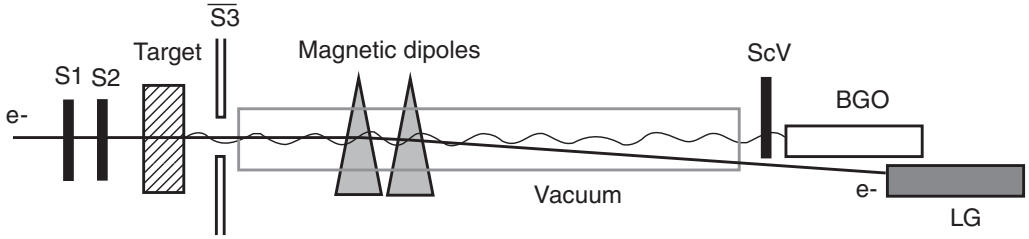

FIG. 1. A schematic drawing of the setup used in the experiment. Two magnetic dipoles, each 2 m along the beam, are used at a low field, $B \simeq 0.16$ T, to reduce the influence of synchrotron radiation in the MeV region. This, combined with the necessity of deflecting the electrons outside the BGO calorimeter, into the lead glass calorimeter, forces a long lever arm. Right in front of the BGO, a veto scintillator SCV was mounted to reject events where the photon has converted or events where an electron may have interacted with the vacuum chamber, generating a shower. The total length of the setup was about 70 m.

front of the BGO. From these measurements we find a Gaussian beam with a standard deviation of $\sigma \approx 12$ mm. We can also use this to determine the beam divergence, since the size of the beam is limited by the Ø9 mm hole scintillator. If it is assumed that the angle made by the direction of the particle and the beam axis is proportional to the distance of the particle from the axis, we calculate a beam divergence of around 0.2 mrad for particles just inside the hole scintillator. This is in good agreement with previous measurements with drift chambers [9,10].

The emitted photons are detected by a BGO calorimeter which is described in Sec. II B. The electrons that only emit a low-energy photon will be detected by a lead glass (LG) calorimeter which is positioned next to and slightly downstream of the BGO detector. If the electrons have emitted a high-energy photon, the electrons are deflected into the vacuum pipe and not detected. To avoid events where electrons hit the BGO, we have positioned a scintillator (SCV) in front of the BGO. Besides measuring the BGO signal we also measure the height of the signal just before an event. This is motivated in Sec. II B.

The data were recorded using an event-based VME system making off-line event selection possible. The count rate was $\simeq 1.6 \times 10^4$ electron triggers $S1 \cdot S2 \cdot \overline{S3}$ per burst, with a burst duration of 9.7 s repeated every 44.4 s, for all targets.

A. Targets

All targets consisted of layers of disk-shaped foils with a diameter of Ø25 mm (except the carbon targets which had a square shape) and different thickness δt. The number of layers N in a target was selected such that the total target thickness $\Delta t = N \cdot \delta t$ would correspond as closely as possible to 105 μm of tantalum which is 2.56% X_0, where X_0 is the radiation length of the target. The choice of total thickness was a trade-off between obtaining an acceptable signal-to-background ratio and keeping multiphoton events at a minimum. The influence of the latter is already substantial at this thickness. Example for 178 GeV electrons, the BH yield is reduced by 15% for a total radiated energy of 1 GeV. Keeping target thicknesses in units of X_0 almost constant makes the contribution from multiphoton events similar in all spectra, as the correction—essentially a shape function—should be a polynomial of the variable $\Delta t/X_0$ [11]. All targets are listed in Table I.

The reference target of aluminum was assembled from 80 disks, each of 25 μm thickness and 1 mm between the individual foils as described in detail in [13]. Since each individual Al foil is significantly thinner than the multiple scattering length of the material, $\ell_\gamma = \frac{\alpha X_0}{4\pi} = 51.7$ μm, this target performs essentially as "single scatterers" i.e. in the BH regime and is a simple, good reference spectrum. The other reference target, tantalum, was chosen since several previous investigations of tantalum are in agreement with theory [13,14].

B. The calorimeters

The main detector in the setup is the BGO calorimeter which is used to measure photons with energies from about 50 MeV to 4 GeV. In addition, a lead glass calorimeter was used to measure electrons with energies above 2 GeV.

The BGO detector has a cylindrical shape with Ø75 mm and 200 mm length which corresponds to $18X_0$. It is coupled to a Photonics XP3330 photomultiplier

TABLE I. Specifications of the targets used. From left to right the columns correspond to the material, the number of foils used, the atomic number of the material, the measured thickness of a single foil, the radiation length [12], and the total target thickness in units of radiation length. Notice that X_0 for carbon and low-density polyethylene (LDPE) is scaled, since the measured density is different from the tabulated density of PDG [12].

Material	N	Z	δt (μm)	X_0 (cm)	$\Delta t/X_0$
LDPE	13	~2	1 mm	48.7	2.67%
C	2	6	2.5 mm	25.4	1.97%
Al	10	13	257	8.897	2.90%
Al ref	80	13	25	8.897	2.25%
Ti	9	22	106	3.560	2.68%
Fe	6	26	80	1.757	2.73%
Cu	5	29	74	1.436	2.58%
Mo	5	42	49	0.9594	2.55%
Ta	1	73	105	0.4094	2.56%

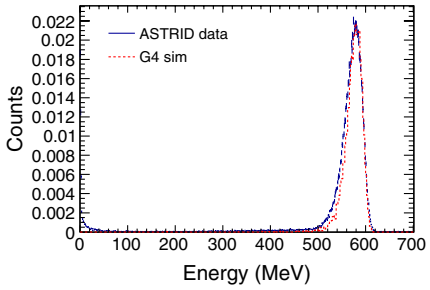

FIG. 2 (color online). The BGO spectrum for 580 MeV electrons obtained from ASTRID compared to a Geant4 simulation of the energy deposit in the BGO crystal.

tube (PMT) and preequipped with a 12 V SCIONIX preamplifer. The detector has been calibrated with an extracted beam from the Aarhus Storage Ring Denmark (ASTRID) where electrons with energies from 100 to 580 MeV are available. This has been done since it is not possible to get an electron beam with an energy below 10 GeV in the North Experimental Area at CERN. It was found that the energy deposit in the BGO was in good agreement with Geant4 simulations in this energy regime (see Fig. 2) and that the detector response was linear (see Fig. 3). The very high χ^2 for the linear fit in Fig. 3 is mainly caused by a slight nonlinearity at energies below 200 MeV and by not including the systematic errors which are difficult to quantify. A high-energy point at 2.6 GeV was measured earlier at CERN with tagged electrons [13]. This measurement showed that the calibration at low-energies could safely be extrapolated to multi-GeV energies and combined with the ASTRID data, this shows that the detector response is linear in the energy regime from 200 MeV up to 2.6 GeV. At energies below 200 MeV the mentioned slight nonlinearity shifts the energies by up to 6 MeV. This does affect the conclusions of this experiment which are not energy sensitive on such a small scale.

Despite the good linearity of the detector, there are several difficulties connected to the BGO detector. In the high-energy environment at CERN, the detector will occasionally be hit by photons with more than 100 GeV. These events are believed to saturate the PMT and affect the detector for a substantial amount of time after the event. We have therefore marked events occurring within 50, 200,

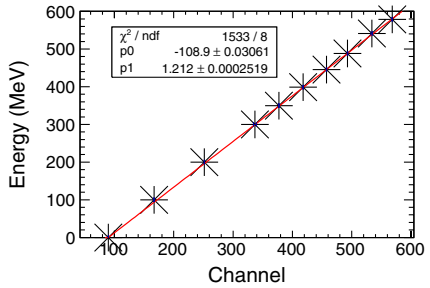

FIG. 3 (color online). BGO calibration made at ASTRID with electrons from 100 to 580 MeV and fitted with a linear function.

and 500 μs after a high-energy event. We have also measured the detector output just before the pulse. This can be used to ensure that the detector has reached its base level, before a new event occurs. Early investigations of the detector led to the conclusion that the PMT should be run at a very low high voltage (HV) of 405 V to minimize saturation. This is significantly below the recommendations by the PMT supplier, 1140 V, based on calibrations with Cs-137 giving 661 keV photons. Nevertheless, our measurements show that this does not affect the linearity of the detector, which has been tested several times.

We have tested the BGO detector in numerous ways to find out if it is well behaved with these nonstandard settings. The goal is to investigate how a high-energy event affects the detector. We mimic this with a short light pulse from a diode, a laserdiode, and an actual pulsed laser. Since the PMT is glued onto the BGO crystal, it is not possible to disassemble the detector and shine light directly onto the photocathode of the PMT. However, it could be accessed from the back by removing an end cap (Photonics XP3330 are no longer available). We used a pulsed nanosecond laser to inject a light pulse into the detector. Surprisingly, the response saturated at signal heights well below the ones observed at CERN. The cause of this is uncertain. A possible explanation could be that the laser only illuminates part of the photocathode, causing a smaller signal than if the full photocathode is illuminated. We have investigated how low-energy events occurring shortly after a saturation event are affected. This has been done with a second light pulse from a diode which is triggered by the laser. The delay between the laser pulse and the diode was varied from 84 to 400 μs and only a small effect was observed, with a reduction in the signal height of about $\sim$10% when the delay was reduced from 260 to 84 μs. No effect was seen when the delay was reduced from 400 to 260 μs. Since the affected data are flagged by the data aquisition system, this effect can be removed from the data in the analysis.

We have investigated the signal height as a function of the HV with a AmBe source giving 4.439 MeV photons. The spectrum measured at a HV of 480 V is plotted in Fig. 4. One can see the pedestal at channel 85, the 4.4 MeV

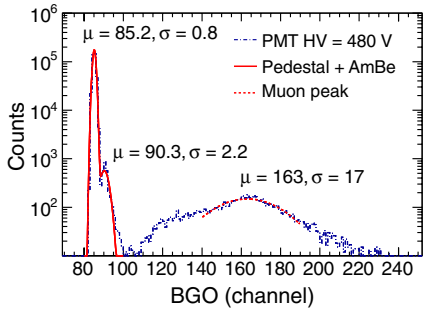

FIG. 4 (color online). The BGO spectrum measured at a PMT HV of 480 V. One can observe the pedestal at channel 85, a 4.4 MeV peak from the AmBe source, and a broad muon peak from cosmics.

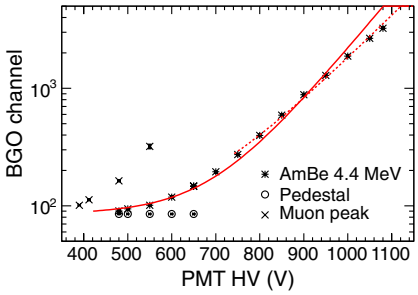

FIG. 5 (color online). The peak channel as a function of PMT HV for the 4.4 MeV peak, the muon peak, and the pedestal. The AmBe data have been fitted to a function describing the PMT amplification in two intervals.

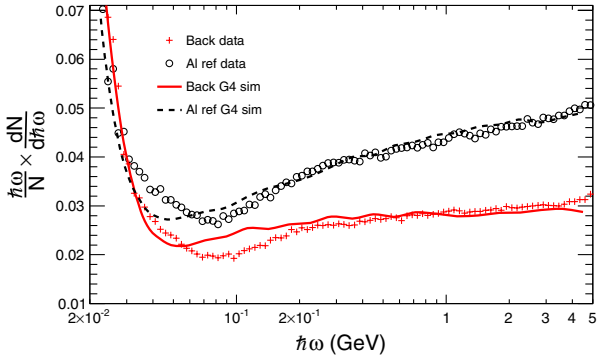

FIG. 6 (color online). Geant4 simulations and measurements of the background radiation and the aluminum reference target. See the text for more details.

peak at channel 90, and a broad muon peak around channel 163. The muon peak is caused by cosmic muons that deposit up to 100 MeV in the crystal. This peak is broad since the detector is cylindrical and the particles therefore traverse different thicknesses of material. The positions of the 4.4 MeV peak, the muon peak, and the pedestal are shown as a function of the HV in Fig. 5. As a simple model of the BGO signal as a function of the PMT HV we use

$$f_{\mathrm{PMT}}(\mathrm{HV}) = a_{\mathrm{ped}} + c \cdot b^{\mathrm{HV}}. \quad (1)$$

$a_{\mathrm{ped}} = 85$ is the pedestal level and b and c are fit parameters. For HV > 700 V there is a very good agreement with a signal doubling every 81 V. If the lower voltages are included in the fit, the agreement is not as good. Nevertheless, the observation of the AmBe signal and the muon peak at low HV indicates that the detector is well behaving, even when operating at a HV significantly below the recommended value.

In conclusion we have tested the BGO detector in various different ways and we did not find any critical effects even though the HV setting for the PMT is substantially lower than the recommendation by the supplier.

III. SIMULATIONS

To compare our measurements to theories we have to make Monte Carlo simulations, since our spectra are affected by multiphoton events, where more photons are emitted by the same electron and detected as one. Such events are easily included in Monte Carlo simulations. Full Geant4 simulations of the background and of the background plus the reference target are shown with the corresponding data in Fig. 6. In this simulation we include the full geometry of the setup, use a Gaussian beam divergence with $\sigma = 0.225$ mrad, a Gaussian beam distribution with $\sigma = 10$ mm and include a background according to our measurements. To find a good agreement between the simulations and the data we have added an extra background of 1.7% X_0 which is probably caused by two beam control scintillators positioned 14 m upstream from the targets (not shown in Fig. 1). In the simulation we store the energy deposit in the BGO, in the lead glass, and in the veto scintillator placed in front of the BGO. We remove all events where more than 0.5 MeV is deposited in the veto scintillator and take into account that only 92% of the particle energy is deposited in the BGO. This fraction has been determined from simulations with monoenergetic beams.

The simulation results for the background and the aluminum reference target are shown in Fig. 6. For the data we have applied a cut removing all events with a hit in the veto scintillator and all events within 500 μs from a high-energy event. The simulations and the data agree very well above 200 MeV and for the low-energy rise below 30 MeV. The magnetic field of the two dipoles is 0.17 T which introduces SR with a critical energy of 3.6 MeV which is well below the low-energy rise. From simulations with and without the LG calorimeter it is clearly seen that the main cause of the low-energy rise is backsplash from the LG. This arises since events where only low-energy photons are emitted are accompanied by a high-energy electron which is only deflected $\sim$7 cm by the two dipoles at the position of the detectors. Unfortunately, the amount of backsplash was not discovered during the experiment. In the intermediate energy region from 30 to 200 MeV there is a dip in the radiation spectrum which is not well understood. Several explanations for this dip have been tested, but all unsuccessful.

Since it has not been possible to accurately reproduce the measured spectrum in the full energy range with the Geant4 simulations (although it is rather close), we have chosen another approach to simulate the radiation spectra, which is significantly simpler and more physically transparent. This method has been used in a previous experiment [15] and only calculates the radiation emitted by the electron and does not track the particle through the setup. It includes a BH radiation background, SR from the magnets, and radiation from the target. We ignore the energy loss of the electron, which can safely be done since we are only interested in events with a low energy loss. However, since we do not track the particle through the setup and therefore do not include the veto scintillator, we have to determine a

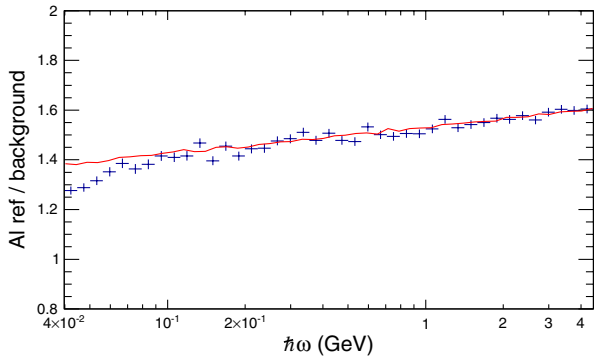

FIG. 7 (color online). The measured (markers) and simulated (line) ratio between the aluminum reference and the background.

detection efficiency. This was not necessary for the Geant4 simulations above. We assume that the efficiency can simply be modeled as a multiplicative factor which varies slightly with energy. We use the ratio of the radiation spectrum from the aluminum reference to the background to determine the amount of material in the background (see Fig. 7). We use these two, since both only include SR and BH radiation, which are well known. By taking the ratio between the two measurements, we remove the detection efficiency, and we can directly compare our data to the simulations. We find that the amount of background material is 3% X_0 which corresponds to the 1.7% X_0 mentioned earlier plus scintillators, mylar foil, air, etc. in the target area. With this background we find the efficiency by dividing the background measurements with the simulations. The result is shown in Fig. 8. We observe a significant efficiency drop from 50 to 200 MeV as was also expected from the Geant4 simulations, but from the ratio (see Fig. 7) it is reasonable to assume that the efficiency corrected simulations are valid down to ~100 MeV, where also the simulations begin to deviate from our measurements. For the 20 GeV data we have used the same method, except that SR is neglected since the critical energy is 0.1 MeV and therefore way below our detection threshold.

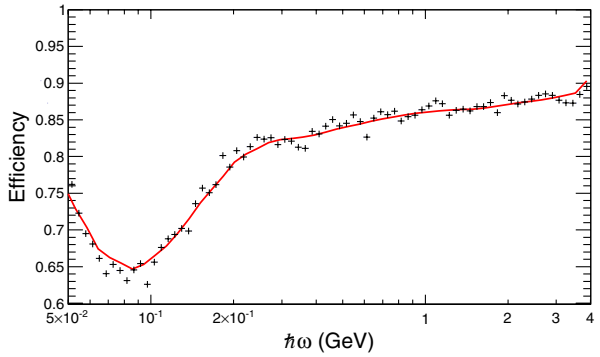

FIG. 8 (color online). Detection efficiency found by dividing the measured radiation background to the simulated as described in the text. The markers are the actual ratio and the line is the smoothed efficiency used in the analysis.

A. Target radiation

For the radiation from the target we use the Migdal [1] cross section calculated with the approximations of Stanev *et al.* [16]. This is considered a standard within the field. However, after the SLAC measurements several other theoretical models were developed. For 178 GeV electrons in carbon and 20 GeV in copper, we also calculate the radiation cross section according to the formalism of Blankenbecler and Drell (BD) [17]. Blankenbecler later refined their treatment of the problem and included an extra correlation term [18]. We have calculated both expressions for the two cases. Alternative descriptions of the LPM effect have also been developed by Baier and Katkov (BK) [19] and Zakharov [20]. The BK description has been calculated for 178 GeV electrons in carbon.

The spectra of the radiated power by 178 GeV electrons traversing a carbon target with a thickness corresponding to 1.97% X_0 are shown in Fig. 9. The differences between the curves are small but worth mentioning. For the BD curve we observe a flattening around 5 MeV. This is related to the finite thickness of the target. If the target thickness is equated to the formation length given by $l_f = 2\gamma^2 c/\omega$ one finds $\hbar\omega = 10$ MeV. This means that for photons with an energy below 10 MeV, one cannot consider the target as semi-infinite and one has to take the size into account. This is naturally incorporated into the BD formalism, but not included in Migdal's formulas. However, this is below our detection limit and does not affect our measurements. We can also ignore transition radiation and dielectric suppression for the same reason. For an experimental investigation of the effects related to the finite target size in the context of bremsstrahlung, the reader is directed to [13]. It is also interesting to notice that it is only the Migdal formulation which shows a small bend around 1200 MeV. The BK curve does not show this but is smooth and otherwise

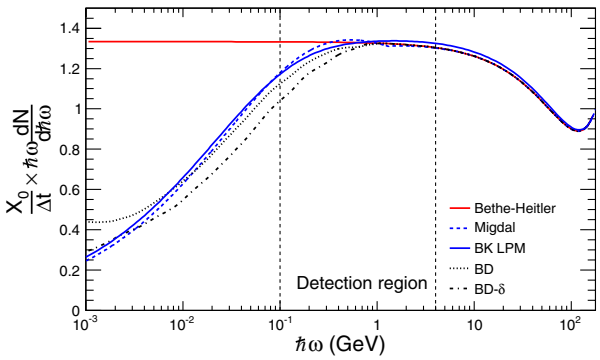

FIG. 9 (color online). Calculated radiation power spectra for 178 GeV electrons traversing a 1.97% X_0 carbon target. The radiation spectra are normalized to the target thickness in units of X_0. The Migdal line is valid for a semi-infinite target and calculated with the approximations of Stanev *et al.* BK refers to the theory of Baier and Katkov. The Blankenbecler and Drell curves (BD and BD-δ) are calculated for a finite size target. The δ refers to formulas in [18] including an extra correlation term.

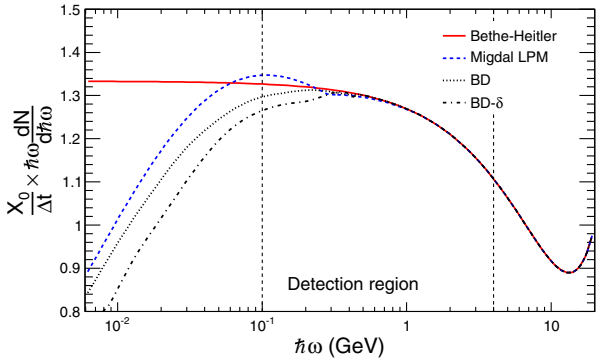

FIG. 10 (color online). Calculated radiation power spectra for 20 GeV electrons traversing a 2.58% X_0 copper target. See caption of Fig. 9 for more information.

very close to the Migdal curve. The BD curve is also very similar to Migdal curve above 10 MeV, but the BD-δ curve is consistently slightly below except for the lowest energies, where the size of the target plays a role and one cannot directly compare them. The 20 GeV spectra in Fig. 10 generally show the same tendencies and the same tendencies are seen for other target materials.

IV. RESULTS AND DISCUSSION

Our results obtained with 178 GeV electrons are shown in Fig. 11. For the reference targets of aluminum and tantalum there is generally a good agreement between the data and simulated values (for Ta only when including the LPM effect, as expected), except perhaps for the lowest (intermediate) photon energies 50–120 (120–600) MeV for the Al (Ta) target where a $\simeq 5\%$ discrepancy is seen. The discrepancy below 100 MeV may be attributed to the influence from the synchrotron radiation and/or backsplash in the BGO as mentioned in Sec. III.

For the LDPE target, the composition is $(CH_2)_xH_2$ and we have calculated curves based on the average Z value of $8/3$ and the average RMS Z value of $\sqrt{6^2+2\times1^2}/3\simeq 2$. The latter corresponds to a Z^2 scaling of the main radiation mechanism. These are hardly distinguishable. Above 200 MeV our data are consistently above the simulations which suggests that the target is slightly thicker than measured or may contain some higher-Z impurity. There is also a slight tendency for the data to be a steeper function of photon energy than the simulated values. For aluminum and titanium there is again good agreement with simulations

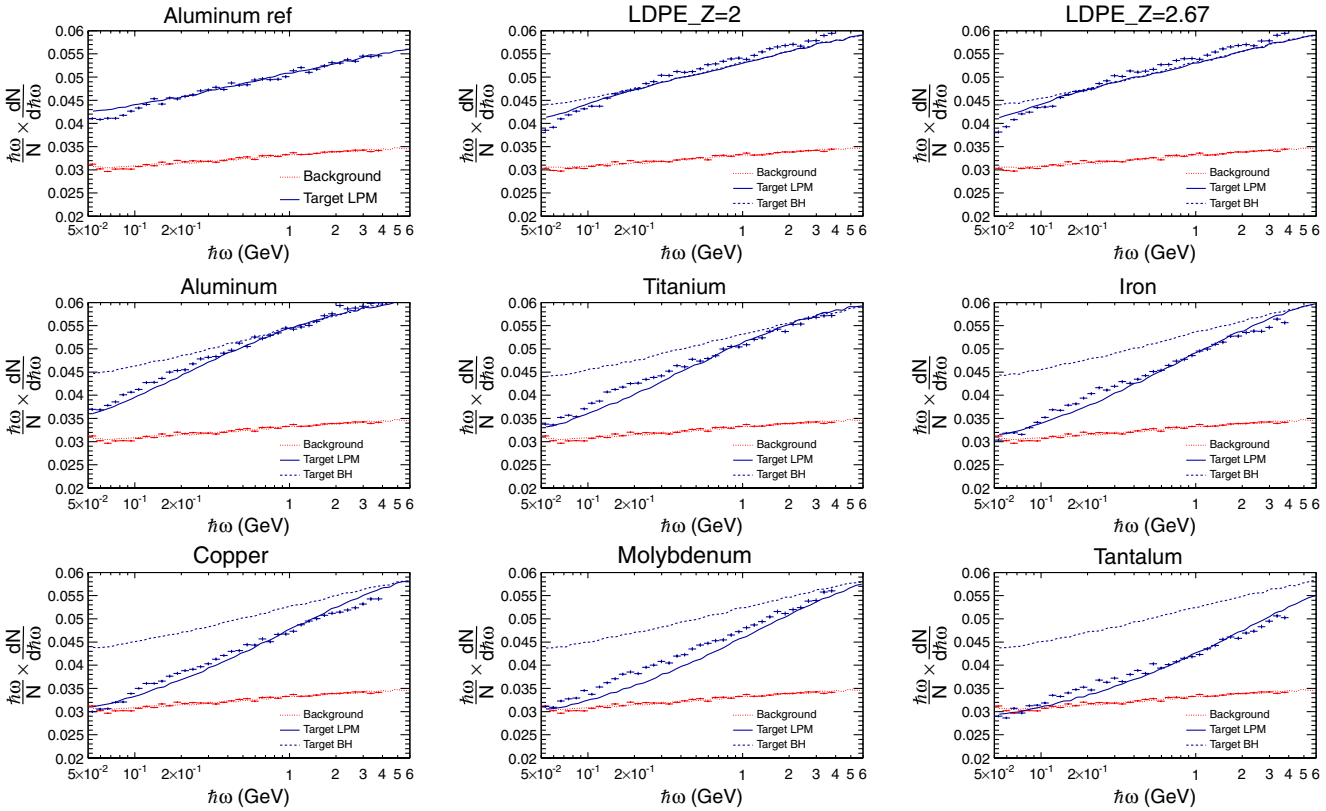

FIG. 11 (color online). Power spectra of radiation emission from 178 GeV electrons penetrating amorphous targets. The spectra are normalized to the number of incoming electrons. The lower, red dotted line shows the simulated contribution from the background, with data points representing the values obtained in the experiment. The middle, blue line shows the simulated contribution from the targets, including the LPM effect, and with data points representing the values obtained in the experiment. The upper, black dashed line shows the simulated contribution from the targets, excluding the LPM effect. Only statistical uncertainties are shown.

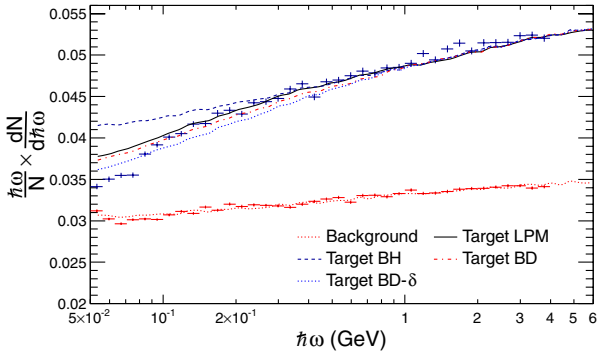

FIG. 12 (color online). 178 GeV electrons in carbon target. See caption for Fig. 11. Additionally, simulations based on the BD and BD-δ theory are included.

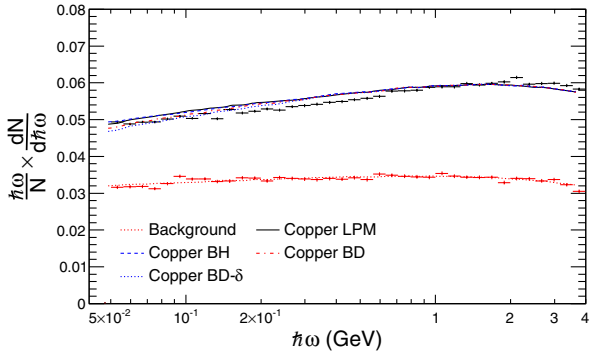

FIG. 13 (color online). 20 GeV electrons in copper target. See caption for Fig. 11. Additionally, simulations based on the BD and BD-δ theory are included.

including the LPM effect, except for a small systematical shift of the experimental values below about 400 MeV. For iron and copper targets—with very similar atomic numbers—the spectra are close to being identical with an indication of a change of slope at the $\simeq 5\%$ level. Finally, for the medium $Z = 42$ molybdenum, the data points are consistently 5%–10% higher than the simulated values including the LPM effect, indicating a systematic error.

For carbon (see Fig. 12) we have also calculated the spectrum for the BD and BD-δ theory. In the energy interval from 100 MeV to 1 GeV where the theories differ we have calculated the χ^2 value. The number of degrees of freedom is 20 and $\chi^2_{\text{Migdal}} = 28$, $\chi^2_{\text{BD}} = 69$, and $\chi^2_{\text{BD-}\delta} = 209$. In other words the data have a preference for the Migdal formula. There is a slight disagreement with the BD curve and the BD-δ curve is consistently below our data.

Our results obtained with 20 GeV electrons in copper are shown in Fig. 13. The appearance of a "kink" in the "raw" spectrum (see Fig. 10) disappears when taking emission of multiphotons and background into account. Thus, an investigation of the potential limitations of the Migdal model in this regime requires very thin targets and a very low background. Our experimental values are generally of the same shape as the simulated spectra, but about 4% lower in magnitude. The reason for this discrepancy is not known, but could be related to contamination of the 20 GeV beam with particles heavier than electrons. Previous measurements have shown that a contamination by nonradiating particles at the 10%–20% level for low energies ($\lesssim 25$ GeV, where synchrotron radiation in the main bends becomes insignificant) can be present if the beam is not carefully tuned. The data cannot be said to have a preference for any of the theoretical models calculated, but are in agreement with all.

Whereas this experiment points toward the inadequacy of the BD-δ theory, we do not have the sensitivity to distinguish between the other theoretical models. It would be preferable to make a more thorough investigation of the effect with an improved setup, better beam conditions, and more statistics. However, our results do not indicate that the Migdal formulation is incorrect.

V. CONCLUSION

We have investigated the LPM effect for 20 and 178 GeV electrons penetrating media of primarily low atomic number. On the scale of about 5% there was no experimentally based reason to suspect that the widely applied model of Migdal should be inadequate, in spite of the statistical nature of the screening function applied and the differing LPM contribution from electrons. Thus, for instance, simulations of extended air showers based on the Migdal formulation should be reliable—for this mechanism and given that the present test can be extrapolated to higher energies—to an accuracy of better than 5%. The carbon data had a preference for the Migdal formula, and the BD-δ curve was consistently slightly below our data. This was in disagreement with previous results on structured targets [15], which had a slight preference for the BD-δ theory. Oppositely, it was in agreement with measurements on thin targets, where the BD-δ theory was also disfavored [21].

[1] A. B. Migdal, Phys. Rev. **103**, 1811 (1956).
[2] P. Gombas, in *Handbuch der Physik*, edited by S. Flügge (Springer, Berlin, 1956).
[3] J. A. Wheeler and W. E. Lamb, Phys. Rev. **55**, 858 (1939).
[4] S. Klein, Rev. Mod. Phys. **71**, 1501 (1999).
[5] P. L. Anthony, R. Becker-Szendy, P. E. Bosted, M. Cavalli-Sforza, L. P. Keller, L. A. Kelley, S. R. Klein, G. Niemi, M. L. Perl, L. S. Rochester, and J. L. White, Phys. Rev. Lett. **75**, 1949 (1995).

[6] P. L. Anthony, R. Becker-Szendy, P. E. Bosted, M. Cavalli-Sforza, L. P. Keller, L. A. Kelley, S. R. Klein, G. Niemi, M. L. Perl, L. S. Rochester, and J. L. White, Phys. Rev. D **56**, 1373 (1997).

[7] H. D. Hansen, U. I. Uggerhøj, C. Biino, S. Ballestrero, A. Mangiarotti, P. Sona, T. J. Ketel, and Z. Z. Vilakazi, Phys. Rev. Lett. **91**, 014801 (2003).

[8] H. D. Hansen, U. I. Uggerhøj, C. Biino, S. Ballestrero, A. Mangiarotti, P. Sona, T. J. Ketel, and Z. Z. Vilakazi, Phys. Rev. D **69**, 032001 (2004).

[9] J. Esberg, K. Kirsebom, H. Knudsen, H. D. Thomsen, E. Uggerhøj, U. I. Uggerhøj, P. Sona, A. Mangiarotti, T. J. Ketel, A. Dizdar, M. M. Dalton, S. Ballestrero, and S. H. Connell (CERN NA63 Collaboration), Phys. Rev. D **82**, 072002 (2010).

[10] K. K. Andersen, J. Esberg, H. Knudsen, H. D. Thomsen, U. I. Uggerhøj, P. Sona, A. Mangiarotti, T. J. Ketel, A. Dizdar, and S. Ballestrero (CERN NA63 Collaboration), Phys. Rev. D **86**, 072001 (2012).

[11] V. N. Baier and V. M. Katkov, Phys. Rev. D **59**, 056003 (1999).

[12] J. Beringer *et al.* (Particle Data Group), Phys. Rev. D **86**, 010001 (2012).

[13] H. D. Thomsen, J. Esberg, K. K. Andersen, M. D. Lund, H. Knudsen, U. I. Uggerhøj, P. Sona, A. Mangiarotti, T. J. Ketel, A. Dizdar, S. Ballestrero, and S. H. Connell, Phys. Rev. D **81**, 052003 (2010).

[14] H. Thomsen, J. Esberg, K. Kirsebom, H. Knudsen, E. Uggerhøj, U. Uggerhøj, P. Sona, A. Mangiarotti, T. Ketel, A. Dizdar, M. Dalton, S. Ballestrero, and S. Connell, Phys. Lett. B **672**, 323 (2009).

[15] K. K. Andersen, S. L. Andersen, J. Esberg, H. Knudsen, R. Mikkelsen, U. I. Uggerhøj, P. Sona, A. Mangiarotti, T. J. Ketel, and S. Ballestrero (CERN NA63 Collaboration), Phys. Rev. Lett. **108**, 071802 (2012).

[16] T. Stanev, C. Vankov, R. E. Streitmatter, R. W. Ellsworth, and T. Bowen, Phys. Rev. D **25**, 1291 (1982).

[17] R. Blankenbecler and S. D. Drell, Phys. Rev. D **53**, 6265 (1996).

[18] R. Blankenbecler, Phys. Rev. D **55**, 2441 (1997).

[19] V. N. Baier and V. M. Katkov, Phys. Rev. D **57**, 3146 (1998).

[20] B. G. Zakharov, JETP Lett. **63**, 952 (1996).

[21] H. D. Thomsen, Ph.D. thesis, Aarhus University, 2010, http://phys.au.dk/fileadmin/site_files/publikationer/phd/Heine_Thomsen.pdf.